Article

Not peer-reviewed version

Tribological and Corrosion Properties of Coatings of Ultradisperse TiB2-TiAl Electrodes with Nanosized Additives Deposited on Ti-Gr2 by Non-Contact Electrospark Deposition

Georgi Kostadinov *, Antonio Nikolov, Yavor Sofronov *, Todor Penyashki, Valentin Mishev, Boriana Tzaneva, Rayna Dimitrova, Krum Petrov, Radoslav Miltchev, Todor Gavrilov

Posted Date: 19 March 2026

doi: 10.20944/preprints202603.1459.v1

Keywords: local electrospark deposition; titanium; wear resistance; corrosion resistance; corrosion characteristics; micropores

 doi:10.20944/preprints202603.1459.v1

Article

Tribological and Corrosion Properties of Coatings of Ultradisperse TiB2-TiAl Electrodes with Nanosized Additives Deposited on Ti-Gr2 by Non-Contact Electrospark Deposition

Georgi Kostadinov [1,*], Antonio Nikolov [2], Yavor Sofronov [3,4,*], Todor Penyashki [1], Valentin Mishev [2], Boriana Tzaneva [4,5], Rayna Dimitrova [2], Krum Petrov [2], Radoslav Miltchev [3] and Todor Gavrilov [6]

[1] Faculty of Industrial Technology, Technical University of Sofia, 1756 Sofia, Bulgaria
[2] Department of Material Science and Technology of Materials, Faculty of Industrial Technology, Technical University of Sofia, 1756 Sofia, Bulgaria
[3] Department of Theory of Mechanisms and Machines, Faculty of Industrial Technology, Technical University of Sofia, 1756 Sofia, Bulgaria
[4] Center of Excellence "Mechatronics and Clean Technology"—Campus Studentski Grad, Technical University of Sofia, 1756 Sofia, Bulgaria
[5] Department of Chemistry, Faculty of Electronic Engineering and Technologies, Technical University of Sofia, 1756 Sofia, Bulgaria
[6] Department of Manufacturing Technology and Systems, Faculty of Industrial Technology, Technical University of Sofia, 1756 Sofia, Bulgaria
* Correspondence: gdkostadinov@gmail.com (G.K.); ysofronov@tu-sofia.bg (Y.S.)

Abstract

The tribological and corrosion behavior of commercial pure titanium - Ti-Gr2 with coatings obtained by mechanized contactless local electrospark deposition (LESD) with a rotating electrode with low pulse energy and an ultradisperse TiB_2-TiAl electrode reinforced with ZrO_2 and NbC nanoparticles is investigated in this work. The current research is driven by the need for improved corrosion resistance of titanium surfaces in automotive components, shipbuilding, aviation, aerospace, petrochemical and many other industrial and domestic areas. The work is a continuation of our previous research, in which the correlations between the electrical parameters of the LESD mode and the relief, roughness, thickness, microhardness, composition and structure of the coatings obtained with this electrode were studied and analyzed. In this work, the influence of the pulse parameters of the LESD process (respectively, the roughness, thickness, composition, structure of the coatings) on the coefficient of friction, abrasive and corrosion resistance of the coatings has been studied and their role in simultaneous protection of titanium surfaces from wear and corrosion has been clarified. Coatings with the presence of newly formed wear-resistant phases and crystalline-amorphous structures, with increased hardness up to 13 GPa, low roughness Ra= 1.5 -2.8 μm, thickness up to 20 μm and minimal structural defects have been formed. By comparing the potentiodynamic polarization curves, polarization resistance, electrochemical impedance and tribological characteristics of the coated surfaces, it has been established that their corrosion resistance increases by more than 2 times and their wear resistance during friction increases by 4-5 times compared to those of the substrate. Appropriate pulse parameters have been defined to allow for uniform coatings with reduced roughness and structural defects, with predictable thickness, roughness and hardness, and with maximized corrosion and abrasive wear resistance.

Keywords: local electrospark deposition; titanium; wear resistance; corrosion resistance; corrosion characteristics; micropores

 doi:10.20944/preprints202603.1459.v1

1. Introduction

In recent decades, due to their unique properties, titanium and its alloys have become desirable materials for numerous industrial applications. One of the main approaches to improve their low hardness and wear resistance to friction and to respond to the progressively growing interests in their use in various industrial sectors is the widespread use of various methods and technologies for applying wear-resistant coatings. However, for the most part, these methods are not always effective and suitable for titanium products, since most of them require complex and expensive technologies and equipment, high costs, and also do not always meet a number of requirements for adhesion, hardness, thickness, roughness, environmental pollution, dimensions and geometry of the processed products, etc. Among these methods, electrospark deposition (ESD) stands out both for its extremely low cost, environmental friendliness, versatility, simple, cheap, compact and portable equipment, easy and flexible technologies and high efficiency at extremely low costs [1–3], as well as for the possibilities of successfully overcoming most of the limitation's characteristic of most of the other methods. ESD can also successfully overcome the limitations in the properties of titanium and titanium alloys, such as low surface hardness, high chemical activity, low wear resistance, and limited oxidation resistance at high temperature [3].

This method allows the application of coatings from any conductive materials with high bonding strength to titanium substrates, the absence of thermal effects and deformation of the titanium substrate, the possibility of local processing of any conductive surface, ultra-fast local heating and cooling [3–5]. This leads to the formation of surface layers with a fine-grained and even amorphous structure and the possibility of changing the characteristics and properties of the coatings in a wide range through the energy parameters of the processing modes and obtaining highly effective physical, mechanical and tribological surface properties, shown in the works [5–7] and those of many other researchers. The high temperatures generated by the occurrence of short-term spark discharges of the order of microseconds and the subsequent transfer of molten electrode material and its mixing with the locally molten material on the substrate surface generate the formation of coatings with new phases and compounds and a strong metallurgical bond with the substrate. The ultra-rapid cooling of the molten anode-cathode mixture in the time between two consecutive discharges causes the formation of metastable phases and fine structures with inclusions of high-hard elements and compounds, and when using certain compositions and electrical process parameters, the formation of amorphous phases is also possible, which is reported in the works [4,8–10]. The ultra-disperse structure of ESD coatings with included crystalline particles embedded in a metal glassy matrix is attractive both in terms of abrasive wear resistance and in terms of corrosion and tribocorrosion protection, which determines the growing interest and applications of the ESD method for strengthening titanium and its alloys, as well as the progressive increase in the number of studies in this direction. However, most of these studies are focused on increasing the hardness and tribological characteristics of the coated surfaces, while improving corrosion resistance is the subject of relatively fewer studies [3,6]. ESD is most commonly used to strengthen and improve the wear resistance of steel surfaces by depositing hard and wear-resistant materials, mainly from hard alloy electrodes based on WC, TiC, TiCN, TiB_2 Cr_2C_3, etc., [1,2,11,12].

It is well known that the corrosion resistance of titanium and its alloys is mainly due to the formation of a titanium oxide film [3,5,6,11]. However, the oxide layers are fragile and usually easily destroyed in the presence of mechanical loads, friction and elevated temperatures, which leads to rapid abrasive wear and corrosion of titanium surfaces. To improve the corrosion resistance of titanium and titanium alloys by ESD, researchers mainly use metals and metal alloys. Cadney et al. [8], Milligan et al. [9], Burkov et al. [10], use aluminum and aluminum alloys, with which they obtain coatings with the presence of amorphous-nanocrystalline structures, with reduced roughness and structural defects and improved corrosion resistance and wear resistance. Ti-Al alloys have been used to improve the corrosion resistance of titanium and its alloys and by other surface treatment methods [13,14], and Kornienko et al. [15] reported on improving the corrosion resistance of titanium in ESD with a palladium electrode. The coatings of metals and metal alloys obtained by these and other

 doi:10.20944/preprints202603.1459.v1

authors, however, have lower hardness (Burkov et al. [10], reported that the microhardness of TiAl coatings on Ti6Al4V alloy is 6.4 - 9.4 GPa) and the wear resistance of these coatings is lower than that when using hard alloy electrodes [16–19]. The corrosion resistance of hard alloy coatings, however, is usually lower than that of coatings of metals and metal alloys due to the presence of increased roughness and structural defects characteristic of hard alloy electrodes. In ESD of titanium surfaces with hard alloy electrodes, the amount of the part transferred from the solid (not completely melted or softened) state of the electrode is relatively high and the coatings usually have higher roughness than that of the substrate, asperities and defects such as pores, microcracks and cavities, which reduce the effect of their abrasive and corrosion ~~wear~~ resistance and limit the practical application of the technology in many industrial and domestic areas, where simultaneous protection against corrosion and frictional wear, or tribocorrosion, is required. Although the increased hardness of hard alloy coatings can partially compensate for their lower corrosion resistance, the difficulty in obtaining smooth and continuous coatings limits the use of this method to improve the corrosion resistance of titanium products.

Although the protection of titanium from corrosion has been the subject of considerable scientific research, to date, no unified concept has been proposed in the literature on the influence of coating materials, coating characteristics, and energy parameters of ESD regimes on the corrosion mechanism and corrosion characteristics of coated surfaces. It is also not fully understood to what extent coatings with improved corrosion characteristics are able to improve the hardness and wear resistance of coated surfaces. The studies of the quality indicators of the surface layers (roughness, uniformity, continuity, microhardness, etc.) made it possible to establish that in order to achieve optimal simultaneous resistance to wear and corrosion, it is necessary to combine contradictory requirements such as hardness, strength and toughness, chemical and thermal resistance, and establish control of the characteristics and properties of the coatings and the correlations between the process parameters, composition, structure, properties and durability of the coated surfaces. The compositions of the coatings must combine sufficient thickness (> 10 μm) [3,15,19,20], strong adhesion [3,6], high hardness, low roughness, a small number of structural defects, and high corrosion resistance.

Despite the existence of many research works, the potential of ESD for corrosion-resistant coating of metals and metal alloys with low surface defects is still not well studied, and the growing need for improved hardness, wear resistance and corrosion resistance of titanium surfaces in automotive components, shipbuilding, aerospace, petrochemical industries and many other areas determines the need for research to create coatings with high corrosion potential, low corrosion density and high corrosion resistance. Therefore, there is a need to continue and expand research aimed at using the easy, environmentally friendly and accessible ESD method to create coatings with reduced roughness and surface defects and effective simultaneous protection against wear and corrosion, which can be a cheap and economically and technically feasible substitute for most of the coatings used at the current stage and to fully utilize its unique advantages to contribute to expanding the application of coated titanium products in various areas under friction and corrosion conditions.

A suitable approach for synergy of high mechanical strength and wear resistance under friction with improved corrosion resistance may be the use of SHS-produced composite ultradisperse electrode materials with nanosized additives, which produce coatings with low roughness and structural defects and a combination of high-hardness, nanostructured and amorphous metal phases [21–23]. In this aspect, the TiB_2-TiAl electrodes with nanosized NbC ZrO_2 additives produced by the authors [23–26] are particularly promising for the development of protective coatings with improved characteristics and abrasion and corrosion resistance. According to the authors [27,28], TiB_2 with its high hardness and melting point (3000 °C) participates in the refinement of the coating microstructure and prevents the propagation of cracks, which creates prerequisites for improving wear resistance and corrosion resistance. Due to its properties, TiB_2 is widely used to improve the properties of composites and coatings applied by various methods: thermal, detonation and plasma spraying [29–31], 3D laser printing [32], ESD [33–36]. The above-cited authors reported a significant improvement in the characteristics and wear resistance of coatings containing TiB_2. The combination of high-

 doi:10.20944/preprints202603.1459.v1

hardness TiB_2 with TiAl alloys [8,9,37] and nano-sized additives is a prerequisite for obtaining uniform coatings with reduced roughness and reduced structural defects. There is a lack of sufficient data in the literature on the use of TiB_2-TiAl electrode materials for coatings on titanium surfaces. In our previous works [38–41], the influence of the electrical parameters of the ESD mode on the relief, roughness, thickness, micro- and nano-hardness, phase composition and structure of coatings on titanium and titanium alloys from a TiB_2-TiAl electrode with nano-sized additives NbC and ZrO_2 was studied and analyzed. It was shown that by using contactless local electric spark deposition (LESD) [41] with low-energy high-frequency pulses and TiB_2-TiAl electrodes, continuous dense and uniform coatings with reduced roughness, fewer structural defects, the presence of pseudoamorphous and nanocrystalline structures, with microhardness up to 13 GPa and with the possibility of predicting and controlling their roughness and thickness by changing the parameters of the LESD regime in the ranges Ra =1.5÷3 μm, δ= 6÷20 μm, respectively.

In this context, the aim of the present work is to investigate the influence of ESD process parameters and thickness, roughness and structure on the tribological and corrosion behavior of coatings deposited on titanium Ti-Gr2 with a TiB_2-TiAl electrode created by SHS, to assess the possibilities for enhancing the corrosion and abrasion resistance of the coated surfaces and to indicate appropriate energy parameters of the ESD process that provide simultaneously increased abrasion and corrosion resistance.

The present work is a continuation, summary and completion (conclusion, finalization) of our previous study [41].

2. Materials and Methods

2.1. Electrode Selection

Ultradisperse electrodes were used, created by the authors [23–26] by self-propagating high-temperature synthesis SHS with a composition of TiB_2-TiAl nano (74%Ti +12%B + 14%Al), dispersive reinforced with 7 % nano-sized ZrO_2 and NbC particle additives, which will be referred to as TiB_2-TiAl for brevity. The electrodes with a diameter of 1.5 mm and a length of 40 mm were obtained by electroerosion cutting from prismatic samples with dimensions of 6 mm × 4 mm × 40 mm.

2.2. Substrate

Commercial pure titanium with the trademark Ti-Gr2 (AISI UNS R R56200 and R50400) in the form of square plates with dimensions of 12 mm × 12 mm × 5 mm was used as the substrate. Model plates were obtained from square bars by electroerosion cutting (EDM) and subsequent grinding to a roughness Ra ≈ 2-2.5 μm.

2.3. Research Apparatus

This work is the first study on the use of ESD process and TiB_2-TiAl electrodes to enhance the abrasion and corrosion resistance of titanium surfaces. To obtain dense and uniform coatings with reduced roughness and minimal structural defects, LESD [42] with a rotating electrode, with automatic maintenance of the discharge distance and controlled speed for applying the coatings along the X and Y axes, was used. The coatings were applied on a mechanized machine type "ELFA" - Sofia, Bulgaria [41,42] with low pulse energy E = 0.005 to 0.045 J, pulse voltage 100 V, current I = 11.2 -24 A, capacitance C = 0.2- 5 μF, pulse duration T_i = 3-20 μs, pulse frequency f = 5–20 kHz at pulse duty cycle 0.1, deposition speed 0.6 mm/s and three passes of the electrode. The process control was implemented by changing the electrical parameters of the mode. The parameters of the deposition regimes that produce uniform, dense coatings with low roughness and surface defects, including amorphous-nanocrystalline structures, were determined based on a preliminary optimization carried out in our previous work [41] and are shown in Table 1.

 doi:10.20944/preprints202603.1459.v1

Table 1. Parameters of the selected modes for LESD.

Designation of samples	Current, I, A	Capacitance C, μF	Pulse duration T_i, μs	Frequency f, kHz	Pulse energy E, J
S1	16.0	4.4	12	8.33	0.025
S2	11.2	0.5	12	8.33	0.013
S3	12.8	0.5	8	12.5	0.013
S4	16.0	2.0	12	8.33	0.020
S5	12.8	4.4	8	12.5	0.020

The parameters of the selected modes in Table 1 are in agreement with the statement of Hassan et al. [36] who use ESD technique with low pulse energy and input power of 40 W for preparation of Ti–TiB–TiB_2 nanostructured coatings on Ti–6Al– 4V substrate, as well as with those in the works [23–26], who use pulses with duration up to 60 μs and low capacity to obtain ultradisperse coatings with amorphous and nanostructured phases.

2.4. Research Equipment and Measurement Methodology

2.4.1. Roughness and Thickness of the Coatings

The average roughness of the coatings - Ra, the root means square roughness Rq; the maximum profile height - Rt and the average value of the 5 highest protrusions and the 5 deepest depressions of the profile - Rz were measured with a profilometer "AR-132B" (Shenzhen Graigar Technology, Co., Ltd., Shenzhen, China) in two mutually perpendicular directions in five sections in five parallel measurements with a measuring length of 2.5 mm. The arithmetic mean values, standard deviation and confidence interval were determined. Strongly differing values were rejected using the Grubbs method.

The thickness δ was measured with an indicator with an accuracy of 0.001 mm. The results are the arithmetic mean value of 5 parallel measurements.

2.4.2. Mechanical Properties of the Coatings

The Vickers microhardness (HV) was measured from above (on the coating) using a "Zwick 4350" hardness tester (Zwick Roell, GmbH & Co., KG, Ulm, Germany) equipped with a diamond prismatic Vickers indenter at a load of 0.2 N for 10 s. The number of parallel measurements was 10. To eliminate the influence of the substrate, the measured hardness was calculated according to the method presented in [43].

The coefficients of friction (μ), tangential force and scratch tests of the coatings under progressively increasing normal load from 0 N to 50 N at a rate of 10 N/mm were determined using the "CSM REVETEST Scratch Macrotester" (Anton Paar GmbH– Headquarters, Graz, Austria) equipped with a Rockwell C diamond indenter with a tip radius of 200 μm. The scratch mark was evaluated using optical methods as well as digital recordings of the coefficient of friction (μ) and tangential force (Ft). Light optical microscopy of the scratch marks was performed using a Nikon microscope (Japan) with a 14-megapixel digital camera adapted to the microscope and used to capture the image.

The friction tests were performed with a "Finger on disc" type tribotester under dry friction with rigidly fixed abrasive particles in planar contact under the following conditions: load 5 N; nominal contact pressure 3.47 N/cm^2; sliding speed 0.239 m/s; type of abrasive surface - corundum No. 1200.

The following wear characteristics were calculated:

Mass wear - as the difference between the initial mass of the sample "m0" and its mass "mi" after a certain number of friction cycles: m=m0−mi, mg. The mass of the samples before and after a given friction path were measured with an electronic balance WPS 180/C/2(RADWAG Poland) with an accuracy of 0.1 mg;

 doi:10.20944/preprints202603.1459.v1

Wear rate - the amount of wear per unit of friction work: I=m/(P.L), mg/Nm, where m is the wear of the solid body for the test time, P - the normal load, L - the friction path travelled;

Wear resistance (reciprocal value of the wear intensity).

- Wear intensity - the amount of wear per unit of friction work, mg/m;

2.4.3. Corrosion Behaviour of the Coatings

The corrosion tests were performed with a PalmSens4 potentiostat-galvanostat, PS-Trace 5.9 software and a classic three-electrode cell with a working electrode from the sample and a counter electrode from a Pt plate. All measurements were performed against a reference electrode: Ag/AgCl/3.0 mol/L KCl (E= 0.210 vs SHE).

A corrosion medium of 3.5 wt. % NaCl was used at a temperature of 20 ±1 °C, without stirring and deaeration. The samples were degreased with acetone, washed with distilled water and dried with warm air.

Comparative electrochemical measurements were performed, including tests using:

- open circuit potential (OCP), which gives a qualitative idea of the activity of the metal system in a corrosive environment;

- electrochemical impedance spectroscopy (EIS), which provides an opportunity for

quantitative characterization of the resistance of the metal system to corrosion when scanning in a frequency range from 10^{-2} to 10^{5} Hz with an AC amplitude of 10 mV;

- potentiodynamic polarization (PDP)/ (CVP) when scanning the potential from -0.5 to 2 V vs Ag/AgCl, to study the active-passive behaviour of the coatings.

Each measurement was carried out in three parallel experiments.

The obtained Polarization dependencies, Nyquist plots, and Bode plots were used to estimate the corrosion potential (Ecorr). The corrosion current density ($\mathbf{j}_{corr}$), the passivation current density ($\mathbf{j}_{pass}$) and the corrosion rate were determined using the Tafel extrapolation method.

2.4.4. Microstructure and Elemental Composition of the Layers

The microstructural, morphological analyses and the elemental distribution in the coatings before and after the corrosion tests were performed with a metallographic optical microscope "Neophot 22" (Carl-Zeiss, Jena, Germany) and a scanning electron microscope (SEM-EDS) "EVO MA 10 Carl Zeiss" with an integrated EDX energy-dispersive X-ray microanalyzer system "Bruker" (Bruker AXS, Karlsruhe, Germany).

The phase composition before and after the corrosion tests was investigated with a Bruker D8 Advance X-ray diffractometer (Bruker AXS, Karlsruhe, Germany) in "CuKά" radiation using the PDF-2(2009) database of the International Centre for Diffraction Data (ICDD).

3. Results and Discussion

3.1. Coating Characterization –Roughness Ra and Thickness, Structure and Micro-Hardness of Coatings

The average values of roughness, thickness and microhardness of the coatings obtained in the present work are shown in Table 2, and Figure 1 shows SEM images of the surface of the coatings deposited in modes 1, 3 and 4. As can be seen, the obtained coatings have high density and acceptable uniformity and repeatability of quality characteristics for practice. Their surface roughness is higher than that of the base but lower than that obtained in traditional methods with vibrating electrodes and higher pulse energy [3–5,8].

Table 2. Parameters of roughness, thickness δ and microhardness HV of LESD coatings from TiB_2-TiAl electrode.

Sample	R_a, μm	R_z, μm	R_t, μm	δ, μm	HV, GPa
S1	3.36	10.94	15.93	19	13.5
S2	2.07	7.53	9.05	11	11.9
S3	1.63	6.39	8.65	9	11.2

 doi:10.20944/preprints202603.1459.v1

S4	2.45	9.05	11.66	16	13.2
S 5	2.57	9.89	13.86	13	12.3
WC-Co8	2.68	10.14	11.33	12	11.8
Ti-Gr2	2.07	5.62	5.67		3.4

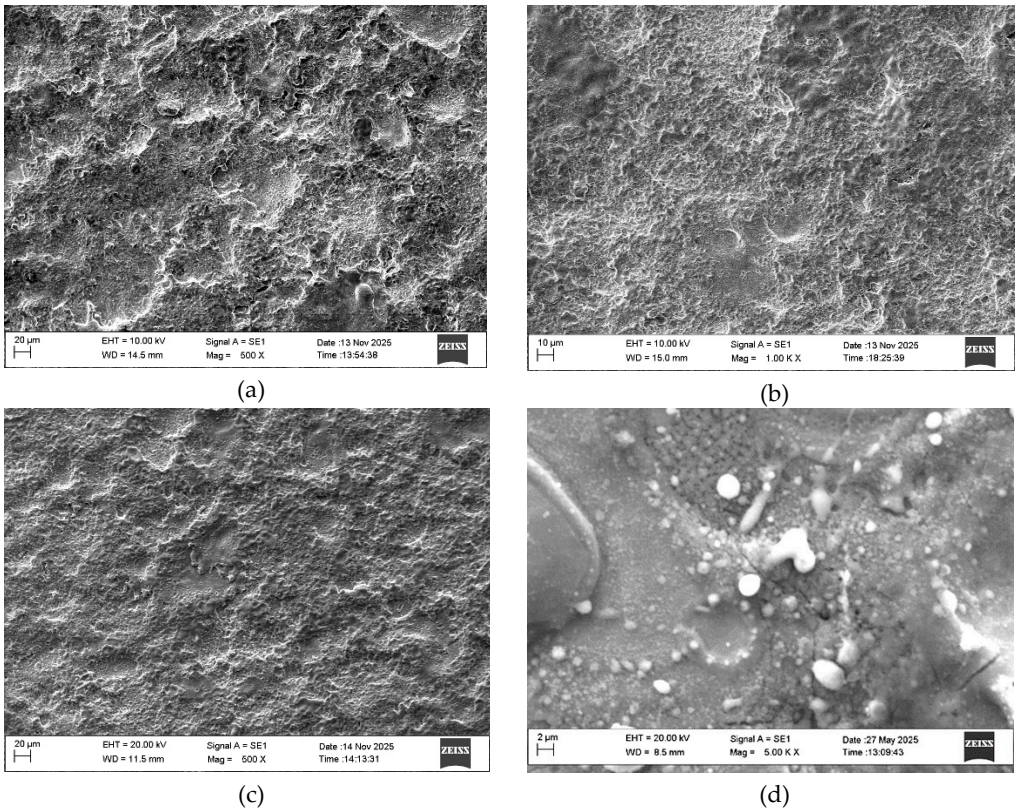

Figure 1. SEM images of the surface of the coatings. (a) Sample S1, (b) Sample S4, (c) Sample S3, (d) Sample S5.

The roughness and thickness of the coatings for the studied energy range vary from Ra 1.6 to 3.36 μm and δ from 9 to 19 μm. The increase in the electrical parameters of the mode (I, C, T_i) (respectively, the pulse energy) leads to an increase in the roughness parameters and the thickness of the coatings. The coatings obtained at current I=11.2, 12.8 and 16 A, capacitance C=0.5 and 2.2 μF and pulse duration T_i=8 and 12 μs - S2, S3 and S4 (Table 2), have a more homogeneous and fine-grained structure, smaller building blocks, higher density and uniformity, and lower roughness than those obtained at the maximum energy used of 0.025 J and capacitance 4.4 μF (Table 1 S1, Figure 1a and S5 Fig. 1d). In LESD with pulse energy E = 0.015-0.02 J, the depth and size of the initial craters on the titanium surface are lower and, accordingly, the surface roughness, the amount of microcracks and the actual contact area during friction are lower, which creates prerequisites for increasing both the wear resistance during friction and the corrosion resistance of the reinforced surface. Also, prerequisites for improved relief and tribological and anti-corrosion properties are created by the presence of nano-sized particles and the increased amount of amorphous and nanostructured phases, registered in [41], as well as the good solubility of the components of the electrode material in the titanium base, as well as the titanium-aluminum alloy, which has a lower melting point than TiB_2 and "spreads" more evenly on the titanium surface. As can be seen from Figure 1, the main components of the coatings are glass-like zones and individual convex relief formations of transferred incompletely melted electrode material, the amount of which increases with increasing pulse energy above 0.02 J, worsening the uniformity and roughness of the deposited surface. Small, lighter irregular dots and fine needle-like formations are also distinguishable. With properly selected modes, LESD can reduce the initial roughness and improve the topography and quality of titanium surfaces, Table 2, S3.

 doi:10.20944/preprints202603.1459.v1

In the SEM images in Figure 1, darker relatively smooth areas are observed, which are most likely the metallic matrix of TiAl/$TiAl_3$. Al-containing intermetallics show smoother morphology upon rapid cooling. $TiAl_3$ is often formed as an intermetallic matrix or around the boride particles. The small oval lighter irregular dots are most likely borides - TiB and TiB_2, which have high hardness. The micron sizes of these dots are typical of secondary precipitated TiB/TiB_2 in Ti and Ti-Al matrix. The fine networks of lighter needle-like formations at the boundaries between the individual areas are likely interparticle phases or oxide phases - Al_2O_3, TiO_x oxides. The slightly larger convex ridged formations are probably TiB_2 (primary), TiC_{1-x}, $TiC_{0.3}N_{0.7}$, or $Ti_{3.2}B_{1.6}N_{2.4}$. Mixed Ti–B–C–N phases are typical for ultradisperse coatings. In these structures, electroerosion craters and smooth areas of the surface are distinguished. At higher magnification, in the case of the 4.4 μF-deposited films (Figure 1d), the presence of individual microcracks, pores and microscopic irregularities is recorded. Among the particles transferred from the electrode, those with a rounded shape are visible. The presence of the spherical shape of the particles (Fig. 1d) indicates that the destruction of the electrode material occurs mainly in the molten state, which is subjected to additional dispersion. This shape of the particles also indicates that the process of electrical erosion of the alloy electrode is carried out mainly from liquid phase. Carbide grains and areas with a glass-like structure are distinguishable (Figure 1 a,b,c,d), whose broadened X-ray diffraction peaks suggest the presence of phases with an amorphous structure. The comparison of the obtained coatings shows that the smoothest and flattest surfaces, with the smallest structural elements and the largest amount of glass-like regions, have the surfaces modified in modes 2, 3 and 4.

The summary of the obtained results allows us to conclude that the use of pulses with lower energy E≤ 0.02 J in LESD leads to the formation of a strengthened surface layer with improved roughness, uniformity and reduced surface defects. The results obtained in Table 2 are similar to those of most studies, where microhardness of coatings from different electrode materials in the range of 6-12 GPa is reported, as well as a large scatter of the results of individual measurements. Similar data are presented by Kornienko et al. [15], who obtained the best results at a low pulse energy E=0.03 J.

Figure 2 shows an optical image of a cross-section of coating S3 at the lowest pulse energy used.

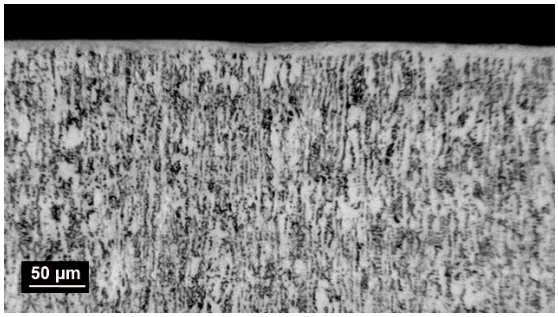

Figure 2. Cros- section microphotographs of microstructure of coatings applied by ESD on Ti-Gr2 at sample S3.

It can be seen that a dense, continuous and uniform coating is obtained. Uniform even layers tightly connected to the substrate with a thickness of up to 8 - 12 μm are visible. The resulting coatings have a compact and uniform microstructure – a white layer almost free of microcracks, which does not mix with the substrate.

From the results obtained (Table 2 and Figures 1,2) it is established that with increasing pulse energy, the parameters of roughness and thickness δ of the coatings monotonically increase. With increasing pulse energy, the diameter of the spark discharge increases, as a result of which the erosion of the electrodes increases. The depth and size of the erosion craters on the cathode increases and, as a result, the roughness increases [6,7,17,34]. The number of microcracks, irregularities and protrusions increases significantly with increasing pulse energy above 0.04 J. And vice versa - reducing the energy leads to obtaining uniform coatings with a finer structure and less roughness,

 doi:10.20944/preprints202603.1459.v1

but also less thickness. In coatings applied with pulse energy up to 0.02 J, the amount of microcracks and irregularities is less. As can be seen from Figures 1 and 2, the use of the TiB_2-TiAl electrode and nano-sized additives at pulse energy up to 0.02 J clearly contributes to the predominant transfer from the liquid phase, improving the relief and reducing the structural defects of the coatings. In the coatings deposited with pulse energy above 0.02 J at a higher magnification, a network of microcracks is observed.

The microhardness values of the coatings processed in mode 1- S1 are the highest, followed by those in S4. The average microhardness values of all coatings are 3-4 times higher than those of the substrate, regardless of the parameters of the LESD regime. The microhardness obtained in the individual measurements varies widely, but its average values for the studied coatings are similar ≈ 11.2 - 13.5 GPa. Based on the analysis, it can be summarized that the high microhardness of the coatings is due both to the presence of high-hard borides, carbides and nitrides in the composition of the coatings, and to the presence of the ultradisperse, reaching amorphous structure of the matrix of titanium and intermetallic phases. The results obtained by us show that the coatings deposited with TiB_2-TiAl electrodes with nano-additives significantly increase the microhardness of titanium alloys and confirm the suitability of these coatings for environments with friction and abrasive wear.

3.2. Phase Composition

As the results of the X-ray diffraction analysis of the coatings presented in our previous work [41] showed, the phase composition of the coatings is similar. The main differences are in the intensity and width of the characteristic phase peaks. Figure 3 and Table 3 show the diffractogram and phase composition of sample S5, with a coating deposited at a capacitance C = 4.4 μF, in which the most pronounced broadening of the characteristic phase peaks is observed at angles 2θ ≈ 35-40°, 53-56°, 61-65°, 70-75°. The broadening of the diffraction peaks of the intermetallic phases and Ti reflects the formation of both solid solutions and nanoscale and amorphous-like structures, which is also confirmed by the reduced crystallite sizes of the individual phases in the range of 15–76 nm (Table 4 and Table 5) and is consistent with the results obtained in [38–41,44,45]. According to these works, as well as according to [3–5,8,17,45], the extremely high cooling rate of the molten microzones 10^5–10^6 °C/s is sufficient to create partial amorphous deposits. Since individual peaks are also present in the broadened zones, it is obvious that the rapidly solidified alloy forms not only amorphous, but also fine-grained crystalline structures. In all coatings, the main phases of the electrode TiB_2, TiAl are observed, but new compounds are also registered that are not present in the electrode and the substrate. In the composition of the LESD layer, the presence of TiB, Al_2O_3, $TiN_{0.3}$, TiCN, Ti_6O, Ti_2O, TiC_{1-x}, $TiC_{0.3}N_{0.7}$, $Ti_{3.2}B_{1.6}N_{2.4}$,TiAl, Ti_2Al, $TiAl_3$, traces of AlB_2, AlN, BN [41], Table 3, which directly affect the microstructure and properties of the coating. The new phases formed in the process of the spark discharges suggest a stronger bond with the base, higher microhardness and therefore higher corrosion and wear resistance.

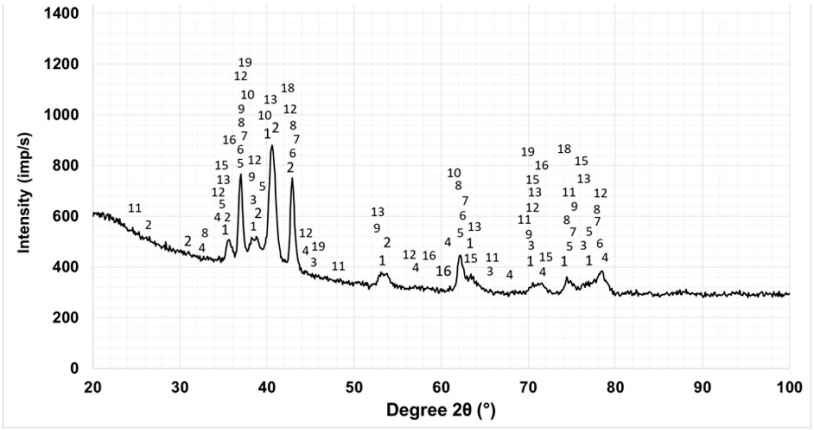

Figure 3. X-ray diffractogram of TiB_2-TiAl coating sample S5 obtained by LESD.

 doi:10.20944/preprints202603.1459.v1

Table 3. Phase composition of the coatings S5.

N	Main phases	N	Phases in small amounts	N	Traces of phases
1	Ti ≈ 32.9 %	**7**	TiN ≈ 4.4 %	**14**	Al ≈ 0.8 %
2	$AlTi_3$ ≈ 2.6 %	**8**	$Ti_{3.2}B_{1.6}N_{2.4}$ ≈ 15 %	**15**	$TiC_{0.7}N_{0.3}$ ≈ 0.8 %
3	AlTi ≈ 1.8 %	**9**	Ti_6O ≈ 3.3 %	**16**	AlN ≈ 2.1 %
4	TiB_2 ≈ 4.5 %	**10**	Ti_3O ≈ 1.7 %	**17**	AlB ≈ 0.9 %
5	$TiN_{0.3}$ ≈ 5.3 %	**11**	Al_3Ti ≈ 2.6 %	**18**	BN ≈ 1.1 %
6	TiB ≈ 8.8 %,	**12**	Al_2O_3 ≈ 2.5 %	**19**	$Al_{2.86}O_{3.45}N_{0.55}$ ≈ 2.4%
		13	Ti_2O ≈3%,	**20**	$TiC_{0.3}N_{0.7}$ ≈ 3.5%

Since each of the recorded characteristic peaks at a specific angle 2θ corresponds to several different phases, the table lists all available phases registered in the presence of a minimum of three diffraction peaks.

Table 4. Crystallite size, of characteristic phases of LESD coatings from TiB_2-TiAl electrode – S5.

Phases	**Ti**	**$TiN_{0.3}$**	**TiN**	**TiC_{1-x}**	**TiC_xN_y**	**TiB**	**TiB_2**	**$TiAl_3$**	**Ti_2O**	**Al_2O_3**	**$Ti_{3.2}B_{1.6}N_2$**	**TiAl**	**Ti_2Al**
Size, nm	39	36	29	26	24	35	68	41	39	51	42	42	32

Table 5. Dimensions of the crystal lattices and crystallites of characteristic phases of LESD coatings from the TiB_2-TiAl electrode.

Coating	**α-Ti,**	**$TiN_{0.3}$**	**$AlTi_3$**	**TiB_2**	**$Ti_{3.2}B_{1.6}N_{2.4}$**	**Ti_2O**	**Al_2O_3**
TiB_2-TiAl-Phases, 2θ	35.7;38.8;40.7;53.5;63;71;75.4;76.8;78.6	35;37.5;39.5;52.2;62.5;69.275.5;77	26.33;31.12;35.65;38.9;39.4;40.8;43.05;53.8	27.7;33.38.8;34.2;44.6;56.9;61.1;68.5;72;78.6	33.36;37;42.95;62.25;74.5;78.5	33.6;35.65;38.45;40.7;53.2;63.75;70.5;76.6;77.15;78.5	19.5;32.1;35.65;37.6;39.2;43.05;44.5;45.6;50;56.7;60.5;66.8;71.4;75.3;78.55
S1, Lattice, Å crystallite size, nm	a= 2.936 c= 4.65232	a=2.969, c=4.78345	a= 5.768 c=4.642446	a= 3.027 c=3.21121	a= 4.23 Å 42	a= 2.9194 c= 4.7130	a= 4.6490 Å c= 12.6870 a= 7.95576
S2, Lattice, Å crystallite size, nm	a=2.949 c=4.684 27	a=2.956 c=4.7736	a= 5.764 c= 4.66436	a= 3.032 c=3.21945	a= 4.2350 Å	a= 2.9194 Å c= 4.7130 Å	Gamma cubic a= 7.932030 a=7.94754
S3, Lattice, Å crystallite size, nm	a= 2.956, c=4.69226	a=2.968, c=4.7843		a= 2.96 Å, c=3.3115	a= 4.2430 Å		a=7.9581 a=7.95458 a= 4.7154 c= 12.851035
S4, Lattice, Å crystallite size, nm	a= 2.945, c=4.68327	a=2.963, c=4.7831	Hexagonal a= 5.768 c= 4.64233	a= 2.96, c=3.3221	a= 4.220 Å	a= 2.9194 Å c= 4.7130 Å 39	Trigonal (hexagonal axes) a= 4.7540 Å c= 12.9820 Å 47

The presence of different phases and structures determines the large differences in the individual measured microhardness values (the lowest measured value is 7 GPa, and the highest 17.7

 doi:10.20944/preprints202603.1459.v1

GPa). The microhardness cannot serve as an accurate comparison of the properties of individual coatings. The higher hardness of the deposits with respect to the base material may be due to the presence of the high-hardness $Ti_{3.2}B_{1.6}N_{2.4}$, $Al_{2.86}O_{3.45}N_{0.55}$, TiB_2, TiB, Al_2O_3, $TiN_{0.3}$, TiCN, as well as the fine-grained ultrafine and amorphous structures with fewer defects [41,44]. The highest values are in the upper part of the layer. In depth, the hardness decreases until it is leveled with that of the base. The microhardness values of the coatings presented in Table 2 are averaged from 10 measurements. Due to the large differences in the measured values, they cannot serve for an accurate comparison of the properties of individual coatings, but they can be used for an approximate assessment in comparisons. Almost all authors report a significant dispersion of the HV values. The obtained surface hardness exceeds the normal value for titanium alloys due to the change in the phase composition and fragmentation of the surface layer structure. The results obtained in Table 2 are similar to most studies, where microhardness of coatings from different electrode materials in the range of 8-12 GPa and a hardening rate of titanium alloys 2.5-4 times are reported.

3.3. Tribological Tests

Figure 4 shows the scratch track, the coefficient of friction (μ) COF, and the tangential force (Ft), of S1, S3, S4 at progressive load scratching mode with normal force range of 0 N to 50 N at a speed of 10 N/mm. Similar data were obtained for the other samples studied.

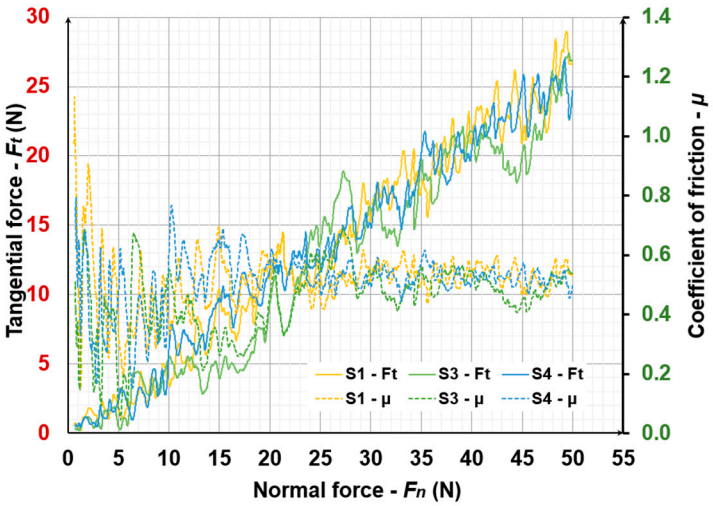

(a)

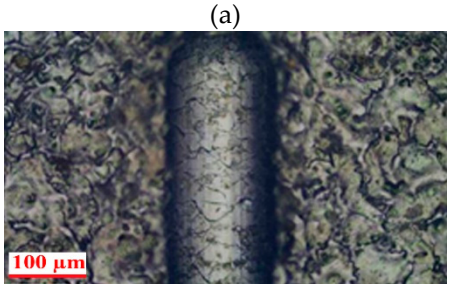

(b)

Figure 4. The coefficient of friction (μ), tangential force (Ft), and the scratch track, of LESD coatings from TiB_2-TiAl electrode S1, S3, S4 at progressive load scratching mode with normal force range of 0 N to 50 N at a speed of 10 N/mm. (a) The coefficient of friction (μ) and tangential force (Ft); (b) A characteristic parts of the track at load 50N of LESD coating of S4.

From the data presented in Figure 4, it can be seen that the values of the friction coefficients μ on the surface of the three samples are very close - about 0.4-0.5 at a load of 50 N. Similarly, the measured values of Ft at maximum load are close and slightly exceed 25 N. The curves of variation of μ and Ft for the three samples have a similar character. The large fluctuations in the signals for S1

 doi:10.20944/preprints202603.1459.v1

are due to the uneven sinking of the indenter with increasing load and the higher roughness of the surface, which is clearly visible in the photographs of the coating (Figure 1a). On the other hand, for S3, the course of variation of μ and Ft with increasing F_N is significantly smoother and more uniform. The friction coefficient of the uncoated sample (Ti-Gr2) is slightly higher 0.55-0.6. As can be seen from Figure 4a, with increasing load, the COF shows an increasing trend, increasing to a load of ≈ 25 N and then remaining almost unchanged up to a load of 50 N. The comparison of the COF values shows that the TiB_2-TiAl coatings show a relatively lower COF, but the differences are relatively small, no more than 10-15 %, despite the significant differences in their roughness parameters.

In S1 (Figure 4b) - at the very beginning of the load application, (albeit fine) cohesive cracks are observed in the scratch test trace. Their size and quantity increase with increasing load. The reason for this is the lower plasticity of the coating. However, the coatings do not show loss of adhesion at a load of up to 50 N. In S2, S3 and S4, no loss of cohesive strength is observed until the end of the test, which indicates good plasticity of the coating.

Figure 5 shows the effect of pulse energy on the wear and wear resistance of coated samples over time, and Table 5 gives the wear intensity of coated samples. ESD coatings produced from a WC–8%Co hard metal electrode were tested as a wear resistance benchmark.

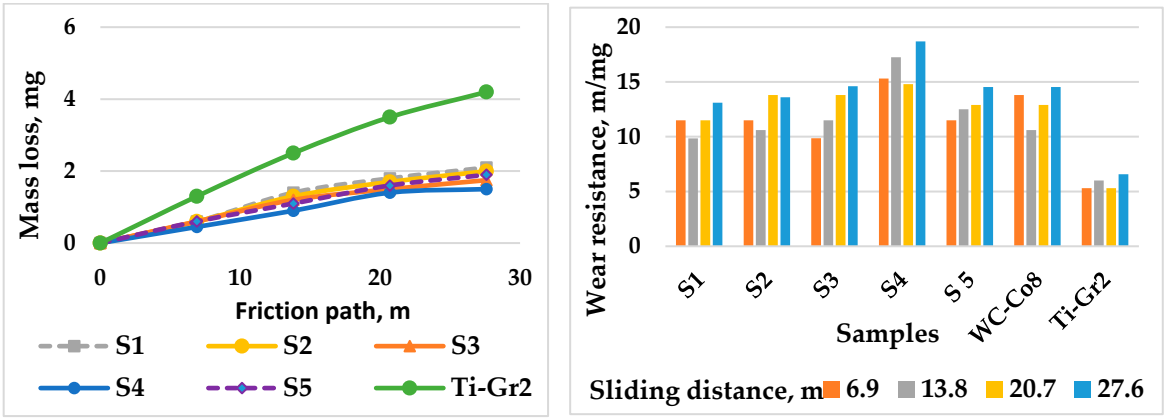

(a) (b)

Figure 5. Mass loss and wear resistance of Ti-Gr2 samples with LESD coatings from TiB_2-TiAl electrode versus sliding distance.

From Figure 5 and Table 6 it can be seen that regardless of the electrical regime parameters used, the coatings from TiB_2-TiAl electrode in dry friction show 2-4 times lower wear, respectively higher wear resistance than that of the titanium substrate. This was expected due to the presence of highly wear-resistant TiB, TiN, $Ti_{3.2}B_{1.6}N_{2.4}$, $TiC_{0.7}N_{0.3}$, $TiN_{0.3}$, TiB_2 and small amounts of AlN, AlB, BN, Al_2O_3, $Al_{2.86}O_{3.45}N_{0.55}$, $TiC_{0.3}N_{0.7}$, TiC_{1-x}, the nanostructured ZrO_2 and NbC additives, as well as the fine-grained ultrafine and amorphous structures with fewer defects. The lowest wear is demonstrated by S4 followed by 3 and 2, and the highest – S1 and S5 coated with capacitance values C=4.4 μF. The comparison of the wear of the coated samples shows that the TiB_2-TiAl electrode coated samples have 1.1 to 1.28 times lower wear than that of the analogous WC-Co8 materials and, accordingly, higher wear resistance. Obviously, the combination of TiB_2 and TiAl and the nanoscale additives of the electrode allow for a reduction in surface defects and roughness, generation of fine-grained and amorphous structures and two- and three-component highly wear-resistant phases which, according to the works [44–46], have a major contribution to the obtained higher wear resistance of the coated surfaces compared to that obtained with WC-Co8 electrodes. The change in the wear rate and wear intensity is similar. Table 7 shows the friction distance of the tested samples under three different wear criteria.

 doi:10.20944/preprints202603.1459.v1

Table 6. Wear intensity of Ti-Gr2 LESD with TiB_2-TiAl electrode.

Samples	Sliding distance, m			
	6.9	13.8	20.7	27.6
	Wear intensity, mg/m.10^{-2}			
S1	8.7	10	8.6	7.5
S2	8.71	9.3	8	6.1
S3	8.6	8.5	7.1	6.3
S4	6.5	6.4	6.7	5.2
S5	6.8	8.2	7.8	7.2
Ti-Gr2	18.8	17.8	16.9	15.6
WC-Co8	7.2	9.4	7.7	6.9

Table 7. Durability of LESD samples at different criteria of wear.

Friction path, m / The durability enhancement factor; Wear, mg	Uncoated Ti-Gr2	LESD with TiB2-TiAl					LESD with WC-Co8
		S1	S2	S3	S4	S5	
1.5	7.2/1	17/2.36	17.6/2.43	21/2.92	28/3.89	18.2/2.57	18.1/2.51
1	5.5/1	11/2	11.5/2.1	12/2.2	19/3.45	13/2.36	12/2.2
0.5	2.2/1	5/2.3	5.2/2.4	5.5/2.5	10/4.54	5.9/2.7	5.85/2.66

From the Table 7 it can be seen that until reaching the wear criterion of 1.5 mg the longest friction path of 28 m, (respectively the highest durability) is shown by S4, and the coefficient of increase in durability compared to that of the substrate is 3.89. The analysis of the friction surfaces showed that the contact surfaces of the coated samples are damaged under the action of abrasive, adhesive and oxidative wear mechanisms. The development and growth of craters from adhesive wear, as well as abrasive wear and chipping of particles from the coating begins from the irregularities and microcracks. In the uncoated samples at a friction path between 7 and 14 m, relatively deep craters and scratches are already present, but in the coated ones the appearance of the same begins after the 20^{th} meter. Therefore, LESD does not prevent wear, but only slows down and reduces its development over time. The higher wear rate of the coated samples at the beginning of the friction process - to the 7^{th} and 14^{th} meter (Table 6) is mainly due to the tensile stresses in the surface layer, which are characteristic of all electrospark coatings and to the detachment of the particles carried by brittle fracture of the electrode, which act as an abrasive. After the removal of the uppermost uneven layer of the coating and the formed abrasive particles from the friction zone, a period of steady state occurs, in which, as a result of the high microhardness of the boride, nitride and carbide phases and the strength of the Ti-Al metal matrix, the wear intensity slightly decreases.

The obtained results show that the influence of the electrode material is also related to the LESD mode. The classical surface microgeometric indicators (R_a, R_z, R_{max}) in this case do not reflect the actual situation of the frictional contact. The coatings of S4 with higher values of R_a, R_z, R_{max} have higher wear resistance than those of S2 and S3 with low roughness. The higher roughness of the coatings obtained in mode 4 -Table 2 suggests a decrease in wear resistance, but this is apparently compensated by the greater thickness and concentration of the wear-resistant phases in the layer, as well as by the higher degree of dispersion and non-equilibrium, i.e. the increase in the pulse energy has led to an increase in the wear resistance of the coatings. The increased wear resistance is apparently provided by the fine-grained and amorphous structure and by the presence of highly wear-resistant compounds in the coatings, which allows to use the full advantages of each component and to provide higher wear resistance of the coating. With a further increase in the pulse energy - S1 and S5, regardless of the greater layer thickness and the higher amount of wear-resistant phases, the wear resistance shows a tendency to decrease. Apparently, the higher values of the roughness parameters, irregularities and structural defects, adversely affect the wear resistance of these

 doi:10.20944/preprints202603.1459.v1

coatings, but the deterioration is compensated to some extent by the greater thickness and the higher content of wear-resistant phases and this leads to relatively small differences in the wear of the two types of coatings. From the obtained results it can be concluded that increasing the pulse energy to 0.02 J and the values of the electrical parameters to I = 16 A, C = 2.2 μF, T_i = 12 μs increases the durability of the coated surface. However, with a further increase in energy, due to the higher roughness and irregularities and structural defects of the coatings, the relative wear resistance gradually begins to decrease. The described wear mechanism, as well as the obtained data on the wear resistance of the coatings are close to those obtained by Koga et al for plasma sprayed amorphous coatings containing TiB_2 [47]. These results show that we have obtained a promising coating with higher performance properties than surfaces coated with classical WC-Co hard alloys. The coatings obtained with lower pulse energy (S2, S3 and S4) reduce the wear intensity compared to uncoated alloys, slow down the development of wear over time and can be used both to reduce surface defects and to increase the durability of rubbing titanium surfaces and parts exposed to abrasion wear.

3.4. Corrosion Tests

The behavior of the TiB_2-TiAl electrode layers in contact with a 3.5% NaCl corrosion medium without external polarization was monitored by measuring the open circuit potential (OCP). All samples demonstrated an open circuit potential (OCP) about 150-200 mV more positive than that of the Ti-Gr2 substrate (Table 8). The OCP values of the samples coated at different regimes are located in a relatively narrow potential range of about 120 mV. They are about 200 mV more positive for all coatings than for uncoated Ti-Gr2 substrate. This result indicates a reduced surface activity after the application of the layers.

Table 8. Corrosion parameters of LESD coatings from TiB_2-TiAl electrode, obtained from polarization dependences taken in 3.5 % NaCl.

Samples	OCP (600s), V	E_{corr}, V	J_{corr}, A/cm²	j_{pass}, A/cm²	R_p, Ohm	CR, mm/year
S1	-0.076	-0.382	1.11×10^{-7}	-	8.58×10^{7}	12.9×10^{-5}
S2	-0.194	-0.336	1.35×10^{-8}	4.76×10^{-6}	3.08×10^{7}	1.57×10^{-5}
S3	-0.143	-0.388	9.25×10^{-9}	5.02×10^{-6}	2.83×10^{7}	1.08×10^{-5}
S4	-0.158	-0.378	1.68×10^{-8}	4.15×10^{-6}	2.06×10^{7}	1.95×10^{-5}
S5	-0.147	-0.170	7.84×10^{-8}	4.24×10^{-6}	3.45×10^{6}	9.11×10^{-5}
Ti-Gr2	-0.380	-0.375	3.97×10^{-7}	-	8.50×10^{5}	4.62×10^{-4}

Electrochemical impedance spectroscopy provides a quantitative characterization of the corrosion resistance of a metal system. The tests were performed at an OCP amplitude of 10 mV with samples with TiB_2 layers and an uncoated Ti-Gr2 substrate. The results are presented in Figure 6 as Nyquist and Bode plots.

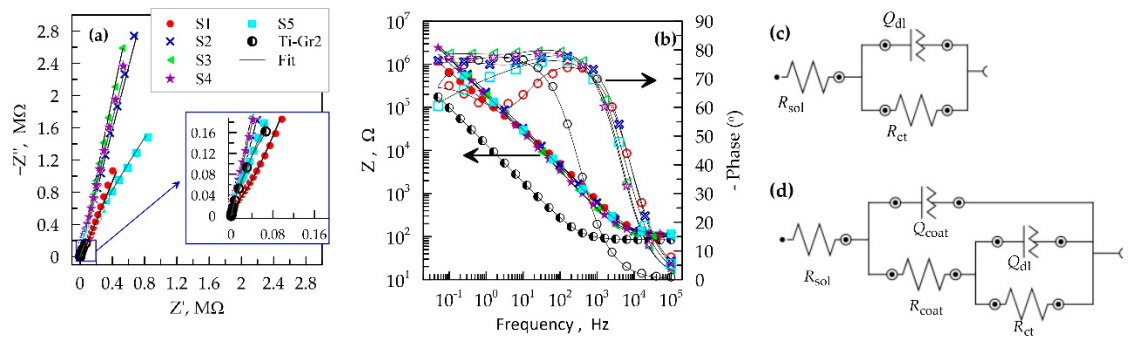

Figure 6. EIS experimental results (symbols) and equivalent circuits for fits (black line): (a) Nyquist plot; (b) Bode plots of impedance module (filed symbols) and phase angles (unfilled symbols); (c) EIS equivalent circuits to

 doi:10.20944/preprints202603.1459.v1

describe the behavior of the Ti-Gr2 substrate; (d) EIS equivalent circuits to describe the behavior of the TiB_2–TiAl electrode layers. The legend presented in Fig. 6a is also valid for 6b.

The Nyquist plot of the Ti substrate is in the form of an incomplete arc (Figure 6a- inset), which is characteristic of metals in a passive state. The increased arc radius indicates improvement of the corrosion resistance and dominance of the capacitive behavior of the coatings. The Nyquist plots (Figure 6a) for S2, S3, and S4 are similar to the strongly pronounced capacitive behavior of protective passive layers. The Bode plots show that in the frequency range 0.01-100 Hz the impedance of the coated samples is about 1 order of magnitude higher than that of the substrate, which gives an additional indication of the effectiveness of the LESD coatings from the TiB_2-TiAl electrode. Therefore, the formed coatings show significantly better barrier ability compared to the uncoated titanium substrate.

The Bode plot of the titanium substrate (Figure 6b) shows a typical behavior of a passive metal surface with a single time constant, which is described by the simplest Randall electrochemical circuit, consisting of a solution resistance R_s in series with a block of electric double layer capacitance Q_{dl} and a charge transfer resistance R_{ct} (Figure 6c). This equivalent circuit has been frequently used to describe the corrosion behavior of titanium and its alloys [13,15,27,49]. In contrast to the substrate, all LESD layers demonstrate a circuit with two-time constants (two maxima in the frequency dependence of the phase shift of the Bode plot). The equivalent circuit in this case is presented in Figure 6d. It has been used in the characterization of titanium alloys and other passive metal systems with highly porous and highly protective passive layers [50,51]. In this case, the circuit is supplemented with the capacitance (Q_{coat}) and the resistance (R_{coat}) of the coating. All capacitances are represented as a constant phase element Q, instead of pure capacitance, since the phase angle does not exceed -80° in the entire frequency range studied (Figure 6). Figure 6 shows a good agreement between the experimental values (represented by symbols) and the fits (black lines) of the used equivalent circuits (Figure 6 c,d). The calculated values of the components in the equivalent circuits are presented in Table 8.

Table 8. Equivalent electrical circuit parameters for TiB_2–TiAl coatings at OCP.

Samples	R_{sol}, Ω	R_{ct}, Ω	Q_{dl}, μS s^n	n_{dl}	R_{coat}, kΩ	Q_{coat}, μS s^n	n_{coat}
S1	104	73.2×10^7	1.400	0.714	85.3	0.791	0.864
S2	94.8	63.0×10^9	0.252	0.740	249	0.697	0.890
S3	102	93.0×10^9	0.177	0.740	384	0.877	0.907
S4	113	43.0×10^9	0.221	0.705	273	0.894	0.899
S5	114	20.9×10^6	0.543	0.560	153	0.837	0.876
Ti-Gr2	84.3	8.92×10^5	14.70	0.872	–	–	–

In general, higher values of R_{ct} are associated with the difficulties of electrochemical reactions (anodic dissolution). All coated samples have one to 4 orders of magnitude higher R_{ct}, which indicates that TiB_2-TiAl coatings can effectively protect the titanium substrate. The highest values of both R_{ct} and R_{coat} are found in S3, which layer was obtained at the lowest pulse energy, capacitance and pulse duration used in this study. The R_{ct} values for S2 and S4 are close to those of S3 and exceed 10^{10} Ω. These layers were also deposited at low to medium pulse energy and capacitance like S3 (Table 1). Samples S1 and S5 deposited at the highest capacitance of 4.4 μF as well as high to medium pulse energy, have two and three orders of magnitude lower R_{ct}, respectively. However, R_{ct} of the titanium substrate is the lowest, with the value remaining below 1 MΩ.

The resistance R_{coat} of samples with TiB_2-TiAl coating increases the total resistance by an additional over 100 kΩ. These results clearly demonstrate the high corrosion resistance of the deposited layers, of which the highest is that obtained in mode 3. The coating obtained by this mode is smooth, uniform and continuous, almost without structural defects and with the most amorphous

 doi:10.20944/preprints202603.1459.v1

and nanoscale phases, as well as with the lowest microhardness of 11.2 GPa and thickness of 9 μm. The lowest R_{coat} have S1 and S5, which are characterized by the highest thickness and microhardness, with the highest content of wear- and corrosion-resistant borides, nitrides and intermetallic phases, but also with the highest roughness, unevenness and structural defects.

Figure 8 presents polarization dependences of Ti-Gr2 samples coated with TiB_2-TiAl electrodes in 3.5 % NaCl. The main corrosion parameters obtained from them are the corrosion potential (E_{corr}), the corrosion current density (J_{corr}), the polarization resistance (R_p) and corrosion rate (CR), and their values are presented in Table 7. These parameters are criterions for the protective properties of coatings. Thus, a more positive E_{corr} usually indicates a tendency towards a passive state as well as higher values of R_p and lower values of J_{corr} and CR of the coated samples indicate better corrosion resistance.

The corrosion potential (E_{corr}) and corrosion current density (J_{corr}) are taken as a measure of the protective characteristics of the coatings. More positive E_{corr} and lower J_{corr} of the coated samples indicate better corrosion resistance compared to the substrate.

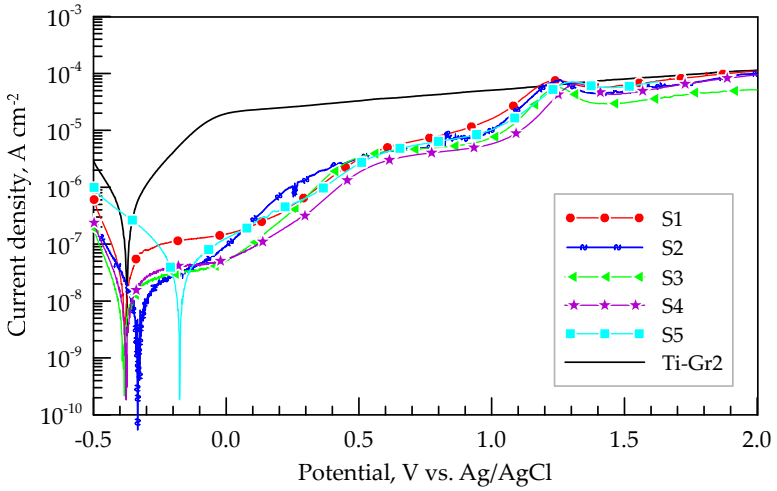

Figure 8. Polarization dependences of TiB_2-TiAl coatings on Ti-Gr2 in 3.5 % NaCl.

Unlike the open circuit potentials, the corrosion potentials of the samples approach that of the titanium substrate Ti-Gr2, with only that of the layer of mode 5 remaining more positive. Most likely, this discrepancy is due to the short cathodic polarization at - 0.5 V vs. Ag/AgCl, performed before starting the polarization test. The corrosion current density J_{corr} of all coated samples is one or two orders of magnitude lower than that of the titanium substrate (Table 7). The lowest values of J_{corr} and CR are again recorded for S3 – two orders of magnitude lower than that of the substrate, followed by S2 and S4. The highest current density is in S1 and S5. These results are consistent with those from the EIS analysis. As presented above (Table 2), the coatings of S3 have lower thickness and roughness parameters, lower microhardness than that of S1, S4 and S5, smaller amounts of high-hard wear-resistant phases and structural defects, but more amorphous and nanoscale phases than those in the coatings deposited with higher pulse energy (capacity C=4.4 μF) S1 and S5, in which the thickness of the coatings and roughness are the highest, and the structural defects such as cracks, micropores and cavities are the most numerous. Apparently, the presence of microcracks suggests access to the surface of the titanium substrate, and the higher roughness and irregularities suggest a larger contact area, which facilitates the flow of current and, accordingly, corrosion.

During anodic polarization in 3.5 % NaCl, the layers undergo complex multi-stage transformation processes in the passive oxide layers. At potentials above 0.5 V vs. Ag/AgCl, the dependences of the layers are superimposed, and at potentials above 1.2 V vs. Ag/AgCl they are aligned with that of the substrate. This behavior indicates a similar composition of the surface layers formed under the different regimes. Neither the TiB_2-TiAl layers nor the Ti-Gr2 substrate show a

 doi:10.20944/preprints202603.1459.v1

tendency to local corrosion, which can be expected for passive metals in the presence of chlorides and high anodic polarization.

Figure 9 presents typical SEM images of coated surfaces after corrosion tests. SEM observations showed that after the corrosion tests on the S3 surface with coatings at the lowest pulse energy used, no particular changes were observed in the surface and relief of the coatings. After the corrosion tests on the surface of S2 and S4 (Figure 9 b,c) the appearance of white dots, threads and needle-like formations is observed. In the secondary electron mode (SE) this is an indication of the formation of phases with lower electronic conductivity, such as aluminum oxides. In addition to similar formations, individual shallow depressions with light borders are also observed on samples S1 and S5, (Figure 9 a,d). These local destructions appear to be the result of the operation of a microcorrosion galvanic cell, in which energy-rich zones are preferentially dissolved.

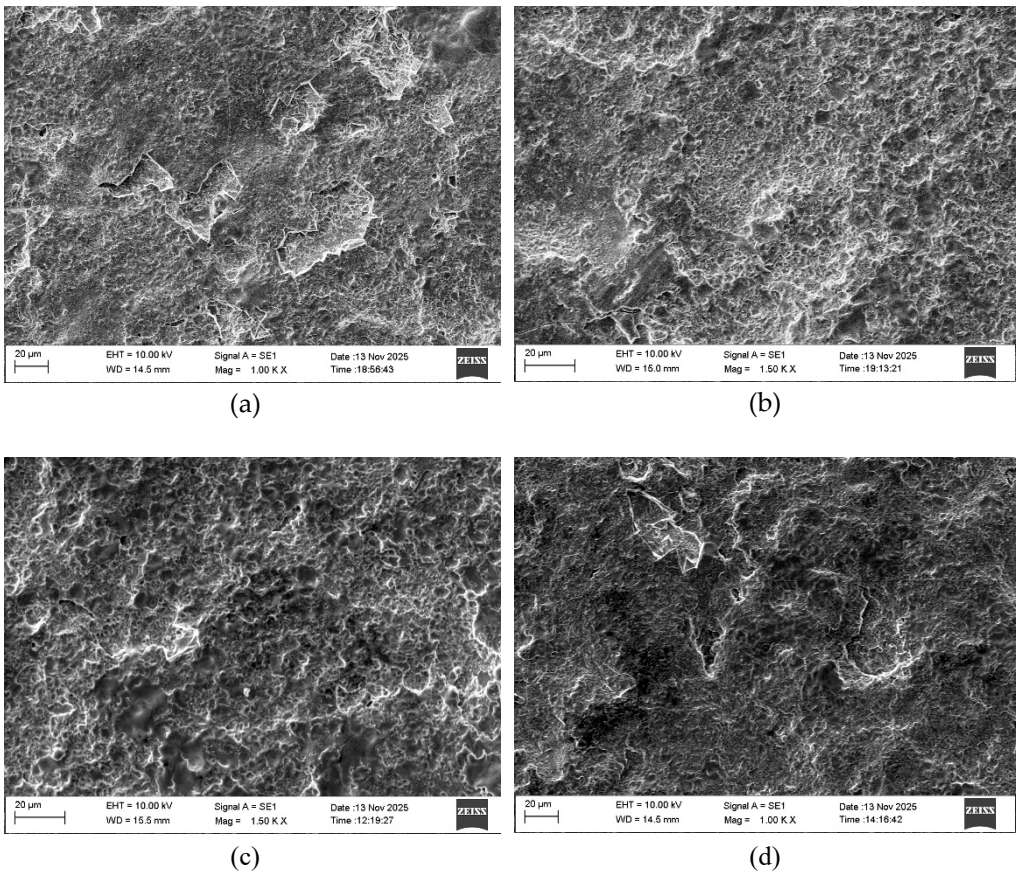

Figure 9. SEM images of the LESD coating surfaces after corrosion tests. (a) Sample S1, (b) Sample S2, (c) Sample S4, (d) Sample S5.

In summary, the results obtained from the corrosion tests show that the protective properties of the coatings of samples S2, S3 and S4 are similar and significantly better than those of samples S1 and S5. The obtained ultradisperse uniform coatings with amorphous-nanocrystalline structures and high-hard and chemically resistant phases such as titanium nitrides, borides and carbonitrides, and ternary dispersion-strengthened ones such as $Ti_{3.2}B_{1.6}N_{2.4}$, $Al_{2.86}O_{3.45}N_{0.55}$ serve as a barrier to the metal with respect to corrosion agents, providing high protection of the titanium substrate. The presence of corrosion-resistant nanosized particles ZrO_2 and NbC also contributes to improving the uniformity of the coating and increasing the corrosion resistance. In addition, the small quantities Ti_2O, Ti_6O and Al_2O_3 synthesized in the LESD process and incorporated in the composition of the coatings, also contribute to the effective protection against corrosion in the aggressive chloride environment. The layers of aluminum oxide on them are impermeable to oxygen and thus protect the titanium.

The obtained results allow us to assume that from the point of view of corrosion resistance, low roughness and uniformity, the presence of amorphous-nanocrystalline structures and the absence of

 doi:10.20944/preprints202603.1459.v1

structural defects are more significant factors than thickness, microhardness and the presence of larger amounts of high-hard boride and nitride phases. Obviously, porosity and structural defects are closely related to both the wear resistance and the corrosion properties of LESD coatings. Of the pulse parameters, the strongest influence is the capacitance, followed by that of t_i on the current I.

The coatings obtained at capacitance values of 4.4 μF have cracks and pores that deteriorate corrosion resistance despite their greater thickness and higher content of high-hard and corrosion-resistant phases. However, despite these defects, local corrosion does not develop even at an anodic polarization up to 2 V. Therefore, it can be assumed that the highest corrosion resistance achieved in these studies is primarily a result of the better uniformity and the smaller amount of pores and microcracks in the coatings deposited in the modes with average pulse energy 0.013 J and 0.02 J. Achieving defect-free coatings by LESD methods is a challenge due to their inherent porosity and microcracks. The present work offers a possible solution to this challenge by using the TiB_2-TiAl electrode and the LESD process in modes with capacitance values up to 2 μF and pulse durations of 8 and 12 μs, making it possible to obtain coatings almost free of structural defects and with many times increased corrosion, abrasion and adhesion resistance.

The coatings of the TiB_2-TiAl–nano electrode material created by self-propagating high-temperature synthesis show up to four times higher wear resistance and up to three orders of magnitude higher corrosion resistance compared to that of the Ti-Gr2 substrate. These results demonstrated that we have obtained promising corrosion resistant coatings, providing corrosion protection of the material and significantly higher performance properties than those of coatings from classical WC-Co hard alloys. The TiB_2-TiAl coatings can be used to increase the durability of titanium surfaces subjected to corrosive and abrasive wear.

4. Conclusions

The coatings obtained by LESD on titanium (Gr2), with a TiB_2-TiAl electrode created by self-propagating high-temperature synthesis, dispersedly strengthened with nanosized additives of NbC and ZrO_2, are uniform with low roughness, increased to 13 GPa microhardness, minimized surface defects and with synthesized new wear-resistant and intermetallic com-pounds such as TiB, $Ti_{3.2}B_{1.6}N_{2.4}$, $TiC_{0.7}N_{0.3}$, $TiN_{0.3}$, TiB_2, AlN, AlB, BN, Al_2O_3, $Al_{2.86}O_{3.45}N_{0.55}$, $TiC_{0.3}N_{0.7}$, TiC_{1-x}, $TiAl_3$ and ultrafine and amorphous-crystally structures.

By using LESD, a continuous and uniform reinforcement layer with fewer defects can be obtained, with improved quality of the coated titanium surfaces and increased mechanical properties as a result of the obtained new wear-resistant compounds and amorphous-crystalline structures. The created coatings achieve a triple effect: reduction of rough-ness and surface defects of the created coatings; increase of wear resistance and service life of the surface-modified products; and increase of corrosion resistance of the modified surfaces.

At pulse energy up to 0.02 J, relatively low capacitance 0.5 -2.2 μF and short pulses of 8-12 μs, a crack-free layer with high adhesion can be obtained, with roughness and thickness that can be changed by changing the pulse energy in the range of roughness Ra 1.6 -2.5 μm, thick-ness 9-16 μm and microhardness 12-13 GPa. It has been experimentally established that coatings applied at lower pulse energy have lower roughness and structural defects, improved surface quality, and reduce the friction coefficient of the coated surfaces by ≈ 10-20 %. They in-crease the wear resistance by friction by 3-4 times, reduce the corrosion rate and increase the corrosion resistance of the modified surfaces by 1-2 orders of magnitude compared to those of the titanium base. Although the coatings obtained by us demonstrate high corrosion potential, low corrosion current density and low corrosion rates, and extremely high corrosion resistance, the corrosion properties and characteristics of ESD coatings on titanium and titanium alloys have not yet been fully studied and deserve attention.

The main factors that ensure an increase in the anti-corrosion properties of coatings are their density and roughness and the ultradisperse and metastable amorphous-crystalline phases, the amount and distribution of which determine the increased corrosion resistance. Research has shown that corrosion occurs from defects such as pores and microcracks. Therefore, con-ducting future

 doi:10.20944/preprints202603.1459.v1

research aimed at improving the uniformity and density of coatings and reducing pores and microcracks is crucial and can significantly improve the corrosion resistance of the strengthened surface.

The study showed that LESD with appropriate electrodes and modes has significant potential to improve corrosion and abrasion resistance and to expand the application of titanium surfaces. The results obtained can serve as a basis for subsequent research aimed at trans-forming ESD into a powerful tool for creating coatings with reduced roughness and structural defects with even higher wear resistance to friction and corrosion.

The coating's protective effect can be further enhanced by improving the continuity of the ESD layer and reducing pores and structural defects, improving the quality characteristics and properties of the coatings and synthesizing new intermetallic and wear-resistant phases and structures, leading to reduced wear and corrosion. Conducting experiments in this direction can also allow the management and optimization of the process for creating coatings with predictable composition, structure, and properties, and the determination of ways to control the composition, structure, and mechanical and operational properties of the reinforced products, and the development of new technologies.

Author Contributions: Conceptualization, G.K., and T.P.; methodology, T.P., Y.S., V.M., A.N., K.P., and G.K.; validation, V.M., K.P., and A.N.; formal analysis, Y.S., B.T., and T.G.; investigation, B.T., V.M., Y.S., R.D., and K.P.; resources, A.N., K.P. and V.M.; data curation, R.M., Y.S., and B.T.; writing—original draft preparation, T.P., and V.M.; writing—review and editing, G.K. and R.D.; visualization, G.K., B.T., T.P., and K.P.; supervision, Y.S.; project administration, Y.S. All authors have read and agreed to the published version of the manuscript.

Funding: This research was funded by financial support from the European Regional Development Fund within the Operational Program "Bulgarian national recovery and resilience plan", procedure for direct provision of grants "Establishing of a network of research higher education institutions in Bulgaria", and under Project BG-RRP-2.004-0005 "Improving the research capacity and quality to achieve international recognition and resilience of TU-Sofia (IDEAS)".

Institutional Review Board Statement: Not applicable.

Informed Consent Statement: Not applicable.

Data Availability Statement: The original contributions presented in this study are included in the article. Further inquiries can be directed to the corresponding authors.

Acknowledgments: The research and preparation of this article were funded by Project BG-RRP-2.004-0005 "Improving the research capacity and quality to achieve intErnAtional recognition and reSilience of TU-Sofia (IDEAS)". The equipment for this study was funded by the European Regional Development Fund under "Research Innovation and Digitization for Smart Transformation" program 2021–2027 and under the Project BG16RFPR002-1.014-0006 "National Centre of Excellence Mechatronics and Clean Technologies".

Conflicts of Interest: The authors declare no conflicts of interest.

References

1. Petrică Vizureanu; Manuela-Cristina Perju; Dragoş-Cristian Achiţei; Carmen Nejneru. Advanced Electro-Spark Deposition Process on Metallic Alloys. Chapter 3 *in Advanced Surface Engineering Research, **2018**.* http://dx.doi.org/10.5772/intechopen.79450
2. Zhang Zhengchuan; Liu Guanjun; I. Konoplianchenko; V. Tarelnyk; Ge Zhiqin; Du Xin. A Review of the Electro-Spark Deposition Technology. *Bull Sumy Nat. Agr. Univ. Ser.: Mechanization and Automation of Production Processes*, **2021**, 2(44), DOI: 10.32845/msnau.2021.2.10
3. Wang, J.; Zhang, M.; Dai, S.; Zhu, L. Research Progress in Electrospark Deposition Coatings on Titanium Alloy Surfaces: A Short Review. *Coating*. **2023**, 13, 1473. https://doi.org/10.3390/coatings13081473
4. Burkov, A.A. The effect of discharge pulse energy in electrospark deposition of amorphous coatings. *Prot. Met. Phys. Chem. Surf*. **2022**, 58, 1018–1027.
5. Mulin, Y.I.; Verkhoturov, A.D.; Vlasenko, V.D. Electrospark alloying of surfaces of titanium alloys. Perspect. Mater. **2006**, 1, 79–85.

 doi:10.20944/preprints202603.1459.v1

6. Mikhailov, V.V.; Gitlevich, A.; Verkhoturov, A.; Mikhailyuk, A.; Belyakov, A.; Konevtsov, L. Electrospark alloying of titanium and its alloys, physical and technological aspects and the possibility of practical use. Short review, *Surf. Eng. Appl. Electrochem*. **2013**, 49, 5, 373-395. DOI: 10.3103/S1068375513050074
7. Podchernyaeva, I.; Juga, A.I.; Berezanskaya, V.I. Properties of electrospark coatings on titanium alloy. *Key Eng. Mater.* **1997**, 132, 1507–1510.
8. Cadney, S.; Goodall, G.; Kim, G.; Moran, A.; Brochu, M. The transformation of an Al based crystalline electrode material to an amorphous deposit via the electrospark welding process. *J. Alloys Compd*. **2009**, 476, 147–151.
9. Milligan, J.; Heard, D.W.; Brochu, M. Formation of nanostructured weldments in the Al-Si system using electrospark welding. *Appl. Surf. Sci.* **2010**, 256, 4009–4016. [CrossRef]
10. Burkov, A.A.; Chigrin, P.G. Synthesis of Ti–Al intermetallic coatings via electro spark deposition in a mixture of Ti and Al granules technique. *Surf. Coat. Technol.* **2020**, 387, 125550.
11. Tarelnyk, V.B.; Gaponova, O.P.; Konoplyanchenko, I.V.; Yevtushenko, N.S.; Herasymenko, V.O. The Analysis of a Structural State of Surface Layer after Electroerosive Alloying. II. Features of Formation of Electroerosive Coatings on Special Steels and Alloys by Hard Wear-Resistant and Soft Antifriction Materials, *Metallofiz. NoveishieTekhnol*. **2018**, 40, 795–815. [in Russian].
12. Burkov, A.A.; Konevtsov, L.A.; Khe, V.K. Formation of electric spark WC-Co coatings with modifying Cr2O3 additives. *Letters on Materials*. **2022**, 12(3), 237-242. https://doi.org/10.22226/2410-3535-2022-3-237-242
13. Liu, Y.; Wang, D.; Deng, C.; Huo, L.; Wang, L.; Fang, R. Novel method to fabricate Ti–Al intermetallic compound coatings onTi–6Al–4V alloy by combined ultrasonic impact treatment and electrospark deposition. *Journal of Alloys and Compounds*. **2015**, 628, 208–212.
14. Riquelme, A.; Torres, B.; Rams, J.; Rodrigo, P. Process–microstructure–property relationships in Ti–Al alloys fabricated by laser directed energy deposition of Ti6Al4V and al powders. *Prog Addit Manuf*. **2026**, 11, 1823–1842. https://doi.org/10.1007/s40964-025-01443-4
15. Kornienko, L.P.; Chernova, G.P.; Mihailov, V.V.; Gitlevich, A.E. Use of the electrospark alloying method to increase the corrosion resistance of a titanium surface. *Surf. Engin. Appl. Electrochem*. **2011**, 47, 9–17. https://doi.org/10.3103/S106837551101011X
16. Penyashki, T.G.; Kamburov, V.V.; Kostadinov, G.D.; Kandeva, M.K.; Dimitrova, R.B.; Nikolov, A.A. Possibilities and prospects for improving the tribological properties of titanium and its alloys by electrospark deposition *Surf. Engin. Appl. Electrochem*. **2022**, 58(2), 135-146. https://doi.org/10.3103/S1068375522020090.
17. Hong, X.; Feng, K.; Tan, Y.F.; Wang, X.; Tan, H. Effects of process parameters on microstructure and wear resistance of TiN coatings deposited on TC11 titanium alloy by electro spark deposition. *Trans. Nonferrous Met. Soc. China*. **2017**, 27, 1767–1776.
18. Levashov, E.A.; Zamulaeva, A.E.; Kudryashov, A.E.; Vakaev, P.V.; Petrzhik, M.I.; Sanz, A. Materials science and technological aspects of electrospark deposition of nanostructured WC-Co coatings onto titanium substrates. *Plasma Processes and Polymers*, **2007**, 4(3), 293– 300.
19. Teplenko, M.A.; Podchernyaeva, I.A.; Panasyuk, A.D. Structure and wear resistance of coatings on titanium alloy and steels obtained by electro spark alloying with AlN–ZrB2 material. *Powder Metall. Met. Ceram*. **2002**, 41, 154–161.
20. Zamulaeva, E.I.; Kuptsov, K.A.; Petrzhik, M.I.; Mukanov, S.K.; Loginov, P.A.; Levashov, E.A. Electrospark Deposition of Hard, Wear-Resistant and Anti-Friction Coatings on γ-TiAl Substrates in a Controlled Gas Environment. *Surf. Engin. Appl. Electrochem*. **2024**, 60, 728–741. https://doi.org/10.3103/S1068375524700315.
21. Manakova, O.S.; Kudryashov, A.E.; Levashov, E.A. On the application of dispersion–hardened SHS electrode materials based on (Ti, Zr)C carbide using electrospark deposition. *Surf. Eng. Appl. Electrochem*. **2015**, 51, 413–421.
22. Kudryashov, A.E.; Levashov, E.A. Application of SHS-electrode materials in pulsed electrospark deposition technology, XV. International Symposium on Self-Propagating High-Temperature Synthesis: Book of Abstracts; IPCP RAS: Chernogolovka, Russia, **2019**; 199–201. Available online:

https://www.ism.ac.ru/events/SHS2019/doc/abstract_shs2019.pdf?utm_source=chatgpt.com (accessed on 24 December 2025

23. Levashov, E.A.; Vakaev, P.V.; Zamulaeva, E.I.; Kudryashov, A.E.; Kurbatkina, V.V.; Shtansky, D.V.; Voevodin, A.A.; Sanz, A. Disperse-strengthening by nanoparticles advanced tribological coatings and electrode materials for their deposition. *Surf. Coat. Technol*. **2007**, 201, 6176–6181. https://doi.org/10.1016/j.surfcoat.2006.08.134.
24. Levashov, E.A.; Malochkin, O.Y.; Kudryashov, A.E.; Glukhov, S.A.; Sviridova, T.A.; Gammel, F.; Zuhentrung, R. Influence of nano-sized powders on combustion processes and formation of composition, structure, and properties of alloys of the system Ti-Al-B. *J. Non-Ferr. Met*. 2003, 1, 54–59.
25. Kudryashov, A.E.; Levashov, E.A.; Aksenov, L.B.; Petrov, V.M. Use of electric spark alloying technology and promising nanostructured electrode materials for improving the life of punching equipment. *Metallurgist*. 2010, 54, 514–522. https://doi.org/10.1007/s11015-010-9332-z
26. Kudryashov, A.E.; Mukanov, S.K.; Sheveyko, A.N.; Rupasov, S.I.; Levashov, E.A. Peculiarities of formation of structure and properties of electrospark coatings on 20X13 steel using SHS-electrodes. *Metallurgist.* ***2025***, 69, 871–881. https://doi.org/10.1007/s11015-025-02007-1
27. Kuptsov, K.A.; Sheveyko, A.N.; Mukanov, S.K.; Bazlov, A.I.; Zaitsev, A.A.; Shtansky, D.V. Effect of boron content and heat treatment on microstructural evolution and tribocorrosion behavior of HEA FeCrNiCoMo-Bx coatings, Materials Today Communications, **2025,** 48, September, 113342. https://doi.org/10.1016/j.mtcomm.2025.113342
28. Lv, X.; Yin, Z.; Yang, Z.; Chen, J.; Zhang, S.; Song, S.; Yu, G. Review on the Development of Titanium Diboride Ceramics. *Recent Progress in Materials.* **2024**; 6(2), 1-48. DOI: 10.21926/rpm.2402009
29. Anuj Bansal , Vikrant Singh , Anil Kumar Singla , Jasdeep Singh , Jonny Singla , Rashad A. Al-Hammadi. Effect of TiB2-B4C reinforcement and laser remelting on the microstructural, mechanical, and tribological performance of HVOF sprayed WC-10Co-4Cr coating, *Colloids and Surfaces A: Physicochemical and Engineering Aspects.* **2026**, 734, 139486, https://doi.org/10.1016/j.colsurfa.2026.139486
30. Zhang, X.; Zhang, S.; Peng, Y.; Geng, L.; Kang, C.; Feng, Z.; Fan, W.; Tan, H.; Lin, X. Process Optimization, Microstructure and Mechanical Properties of SiC + TiB2/AlSi10Mg Composites Fabricated by Laser-Directed Energy Deposition. *J. Manuf. Mater. Process*. **2025**, 9, 404. https://doi.org/10.3390/jmmp9120404.
31. Syrovatka, V. Obtaining composite powder materials and coatings based on titanium diboride. *International Science Journal of Engineering & Agriculture*. **2023**, 2(3), 10–17. https://doi.org/10.46299/j.isjea.20230203.02
32. Kazamer, N.; Valean, P.C.; Pascal, D.; Serban, V.A.; Muntean, R.; Margineal, G. Microstructure and phase composition of NiCrBSi–TiB2 vacuum furnace fused flame-sprayed coatings, *Published in IOP Conference Series Materials Science and Engineering, October 2018, Materials Science, Engineering*, 416, 139816788. DOI:10.1088/1757-899X/416/1/012001
33. Burkov, A.A.; Kulik, M.A.; Bytsura, A.Y.; Krutikova, V.O. Electrospark deposition of boron carbide powder on titanium alloy Ti-6Al-4V, *Letters on Materials*. **2025**, 15(3), 169-175. https://doi.org/10.48612/letters/2025-3-169-175
34. Storozhenko, M.; Umanskyi, O.; Tarelnyk, V.; Koval, O.; Gubin, Yu.; Mikulina, M.; Martsenyuk, I.; Kostenko, O.; Kurinna, T. Structure and Wear Resistance of FeNiCrBSiC–MeB2 Electrospark Coatings. *Powder Metall Met Ceram*. **2020**, 59, 330–341. https://doi.org/10.1007/s11106-020-00166-1
35. Mesut Gökçe; Yusuf Kayali; Şükrü Talaş. The Ceramic Composite Coating (TiC+TiB2) by ESD on Ti6AL4V Alloy and Its Characterization, *Ceramic Sciences and Engineering*. **2020**, 3(1). DOI: 10.24294/cse.v3i1.1136
36. Shafyei Hassan, H.; Salehi, M.; Bahrami, A. Fabrication, microstructural characterization and mechanical properties evaluation of Ti/TiB/TiB2 composite coatings deposited on Ti6Al4V alloy by electro–spark deposition method. *Ceram. Int.* **2020**, 46(10), Part A, 15276– 15284. https://doi.org/10.1016/j.ceramint.2020.03.068Get rights and content
37. Oksana Gaponova; Viacheslav Tarelnyk; Nataliia Tarelnyk; Gennadii Laponog. Investigation of Aluminum Electrospark Alloyed Coatings on Steels, *Metallurgical and Materials Transactions A.* **2025**, 56, 4204-4229. DOI: 10.1007/s11661-025-07908-z

38. Kostadinov, G.; Danailov, P.; Dimitrova, R.; Kandeva, M.; Penyashki, T.; Kamburov, V.; Nikolov, A.; Elenov, Bl. Surface topography and roughness parameters of electrospark coatings on titanium and nickel alloys. *Applied Engineering Letters*. **2021**, 6(3), 89-98. doi:10.18485/aeletters.2021.6.3.1.
39. Penyashki, T.G.; Kostadinov, G.D.; Dimitrova, R.B.; Kamburov, V.V.; Kandeva, M.K.; Valkanov, S.T.; Nikolov, A.A.; Elenov, B.P. Improving Surface Properties of Titanium Alloys by Electrospark Deposition with Low Pulse Energy. *Surface Engineering and Applied Electrochemistry*, **2022**, 6, 580.
40. Penyashki, T.; Kostadinov, G.; Kandeva, M.; Nikolov, A.; Dimitrova, R.; Kamburov, V.; Danailov, P.; Bozhkov, S. Study of the Influence of Coating Roughness on the Properties and Wear Resistance of Electrospark Deposited Ti6Al4V Titanium Alloy. *Tribology in Industry*, **2024**, 46(1), 13-28. doi: 10.24874/ti.1508.06.23.08
41. Kostadinov, G.; Nikolov, A.; Sofronov, Y.; Penyashki, T.; Mishev, V.; Tzaneva, B.; Dimitrova, R.; Petrov, K.; Miltchev, R.; Gavrilov, T. Characteristics and Microstructure of Coatings of Ultradisperse TiB2-TiAl Electrodes with Nanosized Additives Deposited on Ti-Gr2 by Non-Contact Electrospark Deposition, *Materials*, **2026**, 19(3), 572; https://doi.org/10.3390/ma19030572
42. Antonov, B. Device for Local Electric-Spark Layering of Metals and Alloys by Means of Rotating Electrode. U.S. Patent No. 3,832,514, 27 August 1974.
43. Jönsson, B.; Hogmark, S. Hardness measurements of thin films. *Thin Solid Film.* **1984**, *114*, 257–269. https://doi.org/10.1016/0040-6090(84)90123-8.
44. Felix, L.M.; Kwan, C.C.; Zhou, N.Y. The Effect of Pulse Energy on the Defects and Microstructure of Electro-Spark- Deposited Inconel 718. *Metall. Mater. Trans. A.* **2019**, 50(*9*), 4223–4231. DOI: 10.1007/s11661-019-05332-8.
45. Hong, X.; Tan Y.; Zhou C.;H Xu, T., Z. Zhang, Microstructure and tribological properties of Zr–based amorphous nanocrystalline coatings deposited on the surface of titanium alloys by electrospark deposition. *Appl. Surf. Sci.*, **2015**, 356, 1244–1251. DOI: 10.1016/j.apsusc.2015.08.233.
46. Trotsky, M.; Petrovich, S.; Andreeva, V.; Popovich, A.; Zamozdra, M. Synthesis of Ceramics Titanium Compounds by Mechanical Alloying of TiB2-Tin Systems, *Proceedings 30th Anniversary International Conference on Metallurgy and Materials*, May 26 - 28, **2021**, Brno, Czech Republic, 824-828. https://doi.org/10.37904/metal.2021.4204.
47. Koga, G.Y.; Bolfarini, C.; Kiminami, C.S.; Jorge, A.M.; Botta, W.J. An Overview of Thermally Sprayed Fe-Cr-Nb-B Metallic Glass Coatings: From the Alloy Development to the Coating's Performance Against Corrosion and Wear. *J Therm Spray Tech.* **2022**, 31, 923–955. https://doi.org/10.1007/s11666-022-01371-7
48. Brochu, M.; Portillo, J.G.; Milligan, J.; Heard, D.W. Development of Metastable Solidification Structures Using the Electrospark Deposition Process, *The Open Surface Science Journal*, **2011**, 3, 105-114. DOI: 10.2174/1876531901103010105.
49. Nianwei Dai, Lai-Chang Zhang, Junxi Zhang, Qimeng Chen, Maoliang Wu. Corrosion behavior of selective laser melted Ti-6Al-4V alloy in NaCl solution, *Corrosion Science*, **2016**, 102, 484-489. https://doi.org/10.1016/j.corsci.2015.10.041
50. Norbert Radek, Izabela Pliszka, Aneta Gądek-Moszczak, Jarosław Rolek, Jana Petru, Properties of Carbide Electro-Spark Coatings After Laser Processing, *AIP Conference Proceedings*, **2018**, 020024. https://doi.org/10.1063/1.5056287.
51. Socorro-Perdomo, P.P.; Florido-Suárez, N.R.; Mirza-Rosca, J.C.; Saceleanu, M.V. EIS Characterization of Ti Alloys in Relation to Alloying Additions of Ta. Materials, **2022**, 15, 476. https://doi.org/10.3390/ma15020476